

Interpenetrating gels in binary suspensions of DNA nanostars

Cite as: J. Chem. Phys. **157**, 135101 (2022); <https://doi.org/10.1063/5.0117047>

Submitted: 30 July 2022 • Accepted: 05 September 2022 • Accepted Manuscript Online: 06
September 2022 • Published Online: 04 October 2022

 E. Lattuada,  T. Pietrangeli and  F. Sciortino

COLLECTIONS

Paper published as part of the special topic on [Colloidal Gels](#)



[View Online](#)



[Export Citation](#)



[CrossMark](#)

ARTICLES YOU MAY BE INTERESTED IN

[Alternating one-phase and two-phase crystallization mechanisms in octahedral patchy colloids](#)

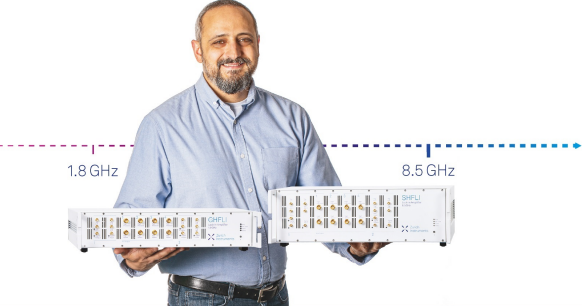
The Journal of Chemical Physics **157**, 134501 (2022); <https://doi.org/10.1063/5.0101529>

[Relating dynamic free volume to cooperative relaxation in a glass-forming polymer composite](#)

The Journal of Chemical Physics **157**, 131101 (2022); <https://doi.org/10.1063/5.0114902>

[Microhydration of the metastable N-protomer of 4-aminobenzoic acid by condensation at 80#K: H/D exchange without conversion to the more stable O-protomer](#)

The Journal of Chemical Physics **157**, 131102 (2022); <https://doi.org/10.1063/5.0119027>



Trailblazers. 

Meet the Lock-in Amplifiers that measure microwaves.

 [Zurich Instruments](#) [Find out more](#)

Interpenetrating gels in binary suspensions of DNA nanostars

Cite as: J. Chem. Phys. 157, 135101 (2022); doi: 10.1063/5.0117047

Submitted: 30 July 2022 • Accepted: 5 September 2022 •

Published Online: 4 October 2022



View Online



Export Citation



CrossMark

E. Lattuada,^{a)} T. Pietrangeli,^{b)} and F. Sciortino^{c)}

AFFILIATIONS

Department of Physics, Sapienza University of Rome, Piazzale Aldo Moro 2, 00185 Roma, Italy

Note: This paper is part of the JCP Special Topic on Colloidal Gels.

^{a)}**Present address:** Faculty of Physics, University of Vienna, Boltzmanngasse 5, 1090, Vienna, Austria.

Author to whom correspondence should be addressed: enrico.lattuada@univie.ac.at

^{b)}**Current address:** Institut Lumière Matière, Université Claude Bernard Lyon 1, 10 Rue Ada Byron, 69100 Villeurbanne, France.

^{c)}**Electronic mail:** francesco.sciortino@uniroma1.it

ABSTRACT

We experimentally investigate the equilibrium gel formation in a binary mixture of DNA nanostars. The binding rules, encoded in the DNA sequence of the nanostar binding ends, are such that each component is able to form only intra-species bonds. Reducing the excluded volume by properly designing the DNA nanostars, we show that two interpenetrating unconnected gels form in the sample on cooling, each of the two forms at a temperature controlled by the selected binding DNA sequence. The dynamic light scattering correlation functions show a non-common three-step relaxation process due to the splitting of the slow relaxation into two distinct decays, each of them reflecting the relaxation dynamics of one of the two networks.

Published under an exclusive license by AIP Publishing. <https://doi.org/10.1063/5.0117047>

I. INTRODUCTION

The spatial coexistence of distinct supramolecular networks is observed in a variety of different physical systems. In the cell, networks of actin, tubulin, and vimentin coexist to provide the functional properties.^{1,2} In polymer physics, double network gels have been shown to significantly affect the viscoelastic properties of the gels.^{3–5} Microgels—finite size particles resulting from the cross-linking of polymers—have also been synthesized with two interpenetrating networks in the attempt to better control the softness and the temperature dependence of the inter-particle interaction.⁶

Designing interpenetrating networks is not an easy task. One needs to avoid demixing phenomena, quite common in polymer physics, as well as density-driven thermodynamic instabilities.⁷ The reward is offered by the possibility to encode the properties of the two networks in the material properties, thus better controlling (and often enhancing) the thermal and mechanical response of the material.

Gel-forming aqueous solutions of DNA nanostars (NSs)—with suitably designed sticky-ends—have been extensively studied in recent years as model systems of patchy colloids. These DNA-made nanoparticles have become the building blocks of numerous

applications, focused on controllable material properties (e.g., equilibrium gels,^{8,9} re-entrant gels,¹⁰ gel isostaticity,¹¹ swapping gels,¹² dendrimers¹³), as well as model systems to investigate liquid–liquid phase-transition in cells,^{14–17} substrates for cell cultures,¹⁸ and modification of cell growth rates.^{19,20} The ability to control the shape, size, functionality, and bond strength of the particle “by design” adds to the versatility of these building blocks. In addition, the close analogy with patchy colloids favors the exchange from theoretical and numerical predictions to laboratory realization.

The particles we investigate in this study are assembled starting from four distinct single-stranded DNA oligomers via a two-step hierarchical self-assembly process. In the first step, the four strands combine to form the desired NS, a star with a flexible central core and four persistent double-stranded arms. In the second step, the single-stranded tips of the arms of the NS (the so-called “sticky sequence”) bind together to form a tetra-coordinate network. The sticky sequence, depending on the number and type of bases of which it is composed, determines the temperature at which the NSs form the network.

The formation of interpenetrating gels of tetravalent patchy colloids has been investigated by de las Heras and co-workers.^{21,22} By analyzing the phase diagram of binary patchy colloids with

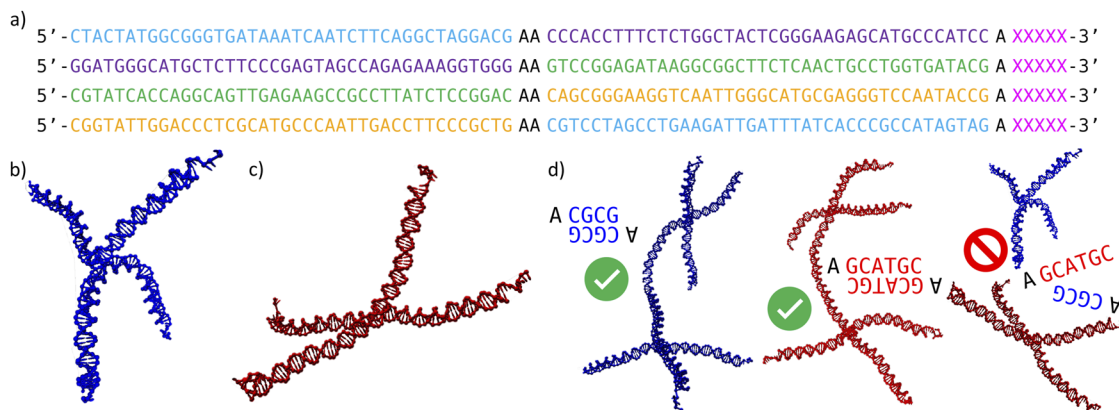


FIG. 1. (a) DNA sequences used in this work. The complementary regions, which selectively hybridize to form the double-stranded NS arms, are highlighted by the same color. The self-complementary sticky-end sequence (highlighted in magenta color), which allows NS-NS interactions, is different for the two NS types. (b) and (c) Representation of the DNA NS of type A (blue) and B (red), respectively, obtained from the self-assembly of the four specific DNA sequences. The configurations have been obtained from oxDNA^{27–29} simulations and the representation has been made using the cogli2 utility.³⁰ (d) NS-NS interactions are only favored between NSs of the same type.

Wertheim theory,^{23,24} for equimolar mixtures of patchy colloids with fixed valence and with no binding between distinct types, they demonstrated the possibility of forming two interpenetrating spanning networks where the two species percolate independently. Given the strong analogy between patchy colloids and DNA-NSs of comparable valence, we attempt here to experimentally realize such a system with the additional aim of demonstrating the design possibilities offered by DNA in controlling the network formation process of each of the two gels.

II. DNA NANOSTARS

We employ two distinct particles (A and B in the following), which differ only in their specific mutual interactions. Each single-stranded DNA oligomer contains properly designed sequences of complementary groups of 40 nucleotides [see Fig. 1(a)]. A well-defined NS is generated by the self-assembly of these strands, which form four double-stranded arms of 40 base pairs [Figs. 1(b) and 1(c)]. Two unpaired adenines, located at the center of each of the four single-stranded sequences composing the NS (resulting in a total of eight unpaired bases, which form the NS core), provide arm flexibility. The self-assembly of the NSs is similar to the one discussed in previous works.^{8,25} Compared to previous studies, the only difference is in the arm length, which we doubled here to reduce the excluded volume and ease network interpenetration. Each arm terminates with a self-complementary, single-stranded sticky sequence preceded by an additional unbonded adenine, which is inserted to ease the linking between different NSs. The sticky-end sequence is different for the A and B NSs and it is designed to favor the NS-NS binding via strand hybridization only between NSs of the same type [see Fig. 1(d)]. To separate the formation temperatures of the two networks, we selected sticky sequences of different lengths. Specifically, one type of NS (A particles) will interact via hybridization of the four-base long CGCG sticky-ends, forming AA bonds; analogously, NSs of type B will form BB bonds via the

hybridization of the six-base long GCATGC sticky tips. Table I reports the hybridization enthalpy ΔH° and entropy ΔS° calculated using the SantaLucia nearest-neighbors model.²⁶ Accordingly, we expect to observe the formation of the B-NSs network around 38 °C and the formation of the A-NSs network around 25 °C.

The probability of forming AB bonds was minimized by reducing the overlap of complementary base patterns in the two sticky sequences (i.e., weak AB bonds can form only by pairing two consecutive complementary base pairs and are thus expected to play a negligible role in the binding process).

III. MATERIALS AND METHODS

A. DNA nanostars

DNA sequences are purchased from Integrated DNA Technologies with polyacrylamide gel electrophoresis purification. The lyophilized samples are initially resuspended in filtered, DNase-free water. For each particle type separately, the tetravalent NSs are pre-assembled by mixing equimolar quantities of the respective single-stranded components. The two mixtures are heated up to 90 °C, incubated for 20 min, and slowly cooled down to room temperature overnight. The NSs annealing is carried out using a Memmert oven.

TABLE I. Sticky-ends hybridization thermodynamic parameters at experimental conditions ($c_{\text{sticky}} = 4c_{\text{NS}} = 320 \mu\text{M}$, NaCl 250 mM). The sticky-ends hybridization enthalpy ΔH° and entropy ΔS° are calculated using the SantaLucia nearest-neighbors thermodynamic parameters.²⁶ The melting temperature is computed from these parameters using the relation $T_m = \Delta H^\circ / (\Delta S^\circ + R \ln(c_{\text{sticky}}))$, where $R = 1.9872 \text{ cal/mol K}$ is the ideal gas constant and c_{sticky} is in mol.

ID	Sequence	ΔH° (kcal/mol)	ΔS° (cal/mol K)	T_m (°C)
A	CGCG	-30.8	-87.4	24.7
B	GCATGC	-43.6	-124.3	37.6

We then prepare 30 μl for each of the three different samples: the first two samples are made of only A and only B NSs, at NS concentration $c_{\text{NS}} = 80 \mu\text{M}$; the third sample is made of both A and B NSs with a 1:1 composition to a total (A + B) NS concentration $c_{\text{NS}} = 160 \mu\text{M}$. The NaCl molar concentration in all samples is fixed at 250 mM. At this value, the Debye–Hückel screening length is about 0.6 nm, to be compared with the diameter of the double helix, of the order of 2 nm, and the arm length of about 15 nm.

The samples are prepared in square borosilicate glass capillaries with an inner size of 2.4 mm (Hilgenberg GmbH). Finally, we cover each suspension with 20 μl of silicone oil and seal the capillaries using UV-curable resin to avoid sample evaporation.

We select the concentration $c_{\text{NS}} = 80 \mu\text{M}$ to avoid any interference in the gelation process from the phase separation that is expected to take place at lower concentrations.²⁵ The absence of phase separation in the samples was checked by thorough centrifugation at 3000g for 48 h, first at $T = 35^\circ\text{C}$ and then at $T = 20^\circ\text{C}$, below the melting temperature of both NSs. At $c_{\text{NS}} = 80 \mu\text{M}$, the volume per NS is $2.1 \times 10^{-4} \text{ nm}^3$, to be compared with the volume of a sphere of radius equal to the NS arm length of $1.4 \times 10^{-4} \text{ nm}^3$.

B. Dynamic light scattering

Dynamic light scattering (DLS) measurements are carried out at a fixed angle $\theta = 90^\circ$ with a custom-made setup consisting of a 633 nm He–Ne laser (17 mW, Newport Corp.) and a multi-tau digital correlator (Brookhaven Instruments) connected to an optical fiber. Samples are immersed in a water bath connected to a thermostat. The actual temperature of the bath near the sample is measured using a thermocouple probe with a $\Delta T = \pm 0.05^\circ\text{C}$ accuracy. For each selected temperature, within the interval $10^\circ\text{C} \leq T \leq 55^\circ\text{C}$ every $\Delta T \simeq 5^\circ\text{C}$, the sample is thermalized for 40 minutes before starting the acquisition. Each measurement lasts between 15 and 90 min, from high to low T . The autocorrelation functions of the scattered intensity $g_2(t)$ are calculated from the correlator output and converted into the field correlation functions $g_1(t)$ using the Siegert relation.³¹

IV. RESULTS

A. Single-component suspensions

We start by discussing, in Figs. 2 and 3, the experimental results obtained for the samples containing only A or only B-type NSs. For both systems, on cooling, $g_1(t)$ develops a two-step relaxation with a slow process that progressively reaches, at low T , the longest experimentally accessible time (100 s). At high T ($T \gtrsim 35^\circ\text{C}$ and $T \gtrsim 45^\circ\text{C}$ for samples A and B, respectively), the correlation functions can be described by a simple exponential decay function, signaling the diffusion process of the NSs and/or small aggregates. With decreasing T , the two-step process develops with well-separated relaxation times. The entire decay of $g_1(t)$ can be fitted as the sum of a fast exponential decay plus a stretched exponential function, the latter accounting for the slower relaxation process,

$$g_1(t) = (1 - C) e^{-t/\tau_f} + C e^{-(t/\tau_s)^{\beta_s}}, \quad (1)$$

where τ_f (τ_s) is the fast (slow) characteristic relaxation time and C and β_s are, respectively, the amplitude and stretching exponent of

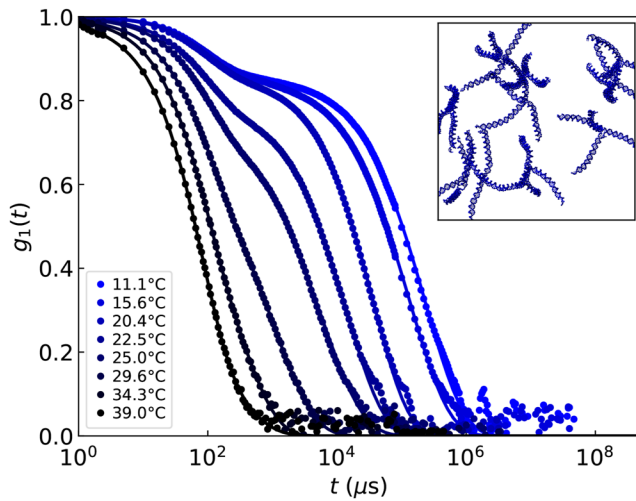


FIG. 2. Field autocorrelation functions (symbols) at different investigated temperatures for sample A. The fit of the data using Eq. (1) is indicated by the continuous lines. In the inset, a pictorial representation of the system is shown.

the slow relaxation process. For each temperature, it is possible to associate an average decay time

$$\langle \tau_s \rangle = \frac{\int_0^\infty dt t e^{-(t/\tau_s)^{\beta_s}}}{\int_0^\infty dt e^{-(t/\tau_s)^{\beta_s}}} = \frac{\tau_s}{\beta_s} \Gamma\left(\frac{1}{\beta_s}\right), \quad (2)$$

where $\Gamma(x)$ is the gamma function. The decay time of the fast relaxation process τ_f is barely dependent on T , and it is not associated with the gel formation process. Hence, it will not be discussed further. By decreasing the temperature, the slow

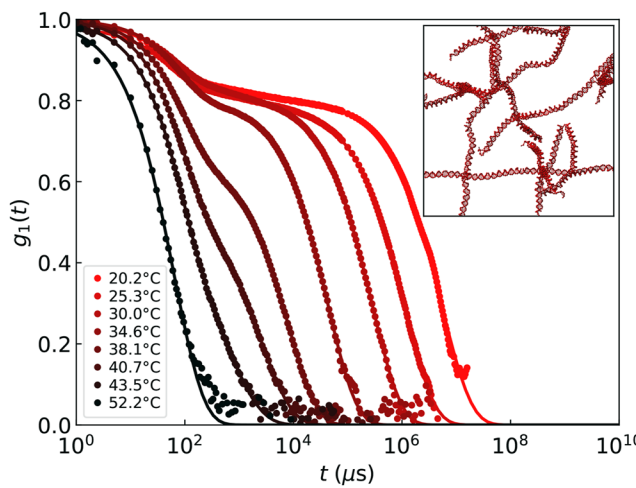


FIG. 3. Field autocorrelation functions (symbols) at different investigated temperatures for sample B. The fit of the data using Eq. (1) is indicated by the continuous lines. In the inset, a pictorial representation of the system is shown.

component—which is related to the dynamics of the network rearrangement—progressively becomes dominant due to the gradual formation of bonds between the NSs, which eventually leads to the development of a fully-bonded state. This process is reflected by the incremental slowing down of the correlation function. The behavior of the correlation functions (shape, time, and temperature dependence) in these single-network samples are fully consistent with previous investigations of equilibrium DNA gels.^{8,32} We refer the interested reader to the original references for further details on the interpretation of $g_1(t)$.

Figure 4 shows the results obtained from the fit of $g_1(t)$. The time $\langle \tau_s \rangle$ [Fig. 4(a)] follows an Arrhenius law for both samples. The slope of $\ln[\langle \tau_s \rangle]$ vs $1/RT$ (where R is the ideal gas constant and T is expressed in kelvin) can be interpreted as an apparent activation enthalpy ΔH . The fit of the data yields $\Delta H = -49.8$ and -72.0 kcal/mol for samples A and B, respectively. The values obtained are roughly 1.6 times the enthalpy associated with the sticky-ends hybridization ΔH° (see Table I), again consistent with previous investigations on similar systems.^{8,32} Upon cooling, the amplitude C of the slow component—which is a measure of the strength of the network—increases, eventually reaching a plateau when all bonds are formed [Fig. 4(b)]. The stretching exponent β_s [Fig. 4(c)] remains almost constant within the whole temperature range for both A and B systems.

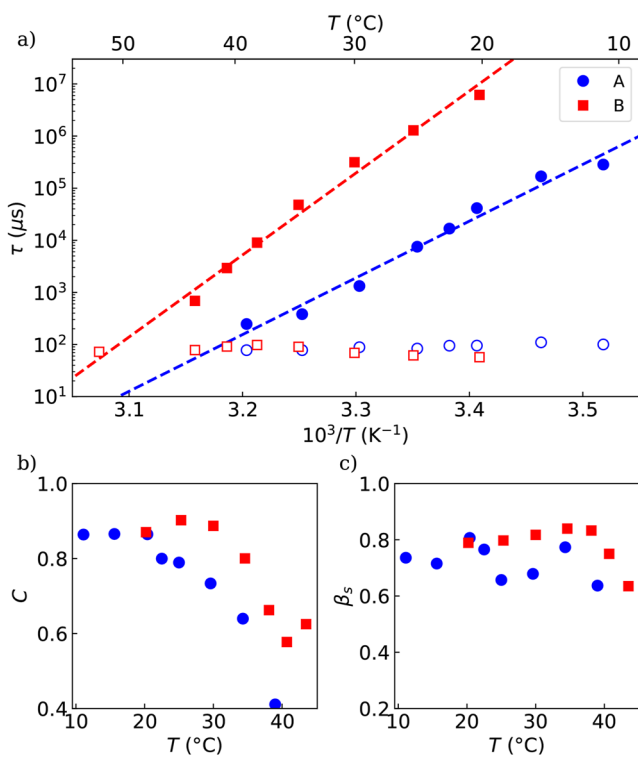


FIG. 4. Fit results for samples A (circles) and B (squares). (a) T dependence of the fast τ_f (open symbols) and average slow (τ_s) (full symbols) relaxation rates. The dashed line is the fit of $\langle \tau_s \rangle$ to the Arrhenius function. The amplitude and stretching exponent of the slow relaxation process are shown in panels (b) and (c), respectively.

B. Two-component mixture

We proceed now by inspecting the experimental results obtained on the equimolar mixture of A and B particles (sample AB in the following). As discussed in Sec. III, the DNA concentration of this sample is twice the one that characterizes both the single-network samples previously discussed. Thus, each component has exactly the same concentration as before, and the mixture sample—in an implicit solvent context—can be thought of as the “sum” of the two previous samples.

In Fig. 5, we show $g_1(t)$ obtained at different T s. As in the case of the single-component samples, the correlation functions decay to zero within the experimentally accessible time window (100 s), confirming the ergodicity of the sample. We expect the B-NSs network to form before the A-NSs network (i.e., at a larger temperature), due to the different melting temperatures of the selected sticky sequences.

Indeed, at $T \approx 40$ °C, the correlation function shows only one slow relaxation process, with a $\langle \tau_s \rangle$ similar to the one observed at the same temperature in the pure B sample. For $T \lesssim 40$ °C, a third relaxation process appears, mirroring the formation of the network of A-NSs.

Here, $g_1(t)$ can be fitted as the sum of a fast exponential decay plus *two* stretched exponential functions, accounting for the two distinct slow relaxation processes,

$$g_1(t) = (1 - C_A - C_B) e^{-t/\tau_f} + C_A e^{-(t/\tau_{s,A})^{\beta_{s,A}}} + C_B e^{-(t/\tau_{s,B})^{\beta_{s,B}}}, \quad (3)$$

where $\tau_{s,B} > \tau_{s,A}$. The symbols used here mirror the ones of Eq. (1), with the addition of a label for the two slow components. As before, the slow relaxation dynamics can be quantified by the average decay time [see Eq. (2)], where τ_s and β_s are replaced by $\tau_{s,A/B}$ and $\beta_{s,A/B}$, respectively.

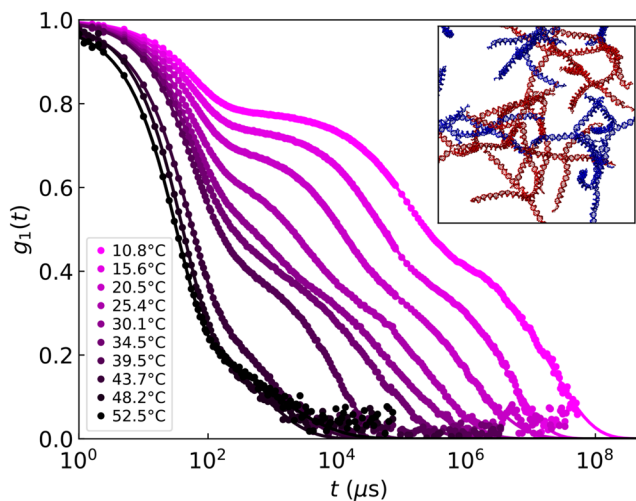


FIG. 5. Field autocorrelation functions (symbols) at different investigated temperatures for sample AB. The fit of the data using Eq. (3) is indicated by the (almost invisible) continuous lines. In the inset, a pictorial representation of the system is shown.

To visualize the different effects on the A and B components in the binary mixture, it is useful to compare the slow component of $g_1(t)$ for the single networks and for the AB sample at the same temperature. To do so, we capitalize on the modeling of the data provided by Eq. (3) to single out only the slow process components. Figure 6 shows, for $T \approx 20^\circ\text{C}$, the reconstruction of the slow component of $g_1(t)$ of the single networks and of the AB sample separated for the A and B parts, when the amplitudes are all renormalized to one (i.e., C , C_A , and $C_B = 1$). The figure clearly shows that the presence of the additional network speeds up the restructuring dynamics of both networks.

To check if the coexistence of the two networks has the sole effect of speeding up the dynamics of the two components or also modifies the activation enthalpy, we then inspect the temperature dependence of the fit parameters for the binary mixture, as shown in Fig. 7. The fast decay time barely depends on T and coincides with the value measured in the single-component samples, so it is not discussed further. Next, we examine the network formation process of the A-NSs—the ones with the weaker sticky sequence—in the AB sample, which is characterized by faster network restructuring. We find that $\langle \tau_{s,A} \rangle$ follows an Arrhenius behavior with an activation enthalpy of about $\Delta H = -44.0 \text{ kcal/mol}$, which is slightly lower than (but very similar to) the value obtained for the pure A sample of -49.8 kcal/mol (see Sec. IV A).

The network formation process of the B-NSs in the AB sample, however, displays a very different temperature dependence. For $35^\circ\text{C} \lesssim T \lesssim 45^\circ\text{C}$, tentatively before the onset of the formation of the A-NSs network, $\langle \tau_{s,B} \rangle$ is compatible with an Arrhenius law with an activation enthalpy very similar to the one measured for the pure B sample. At low temperatures, however, $\langle \tau_{s,B} \rangle$ follows a *different*

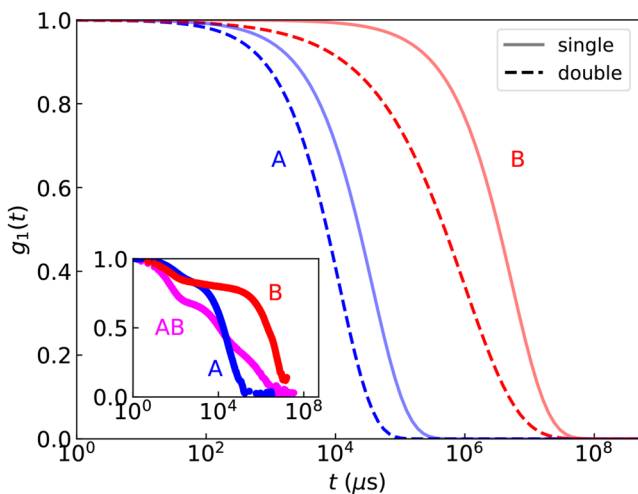


FIG. 6. Comparison of the slow relaxations measured at $T \approx 20^\circ\text{C}$ for the three samples. To better highlight the change in the restructuring dynamics, we reproduce only the slow decay process as modeled by the stretched exponential functional fit, $\exp[-(t/\tau_s)^{\beta_s}]$ with amplitude scaled to one, using the appropriate best fit value for τ_s and β_s obtained from the measured $g_1(t)$ shown in the inset. Here, solid lines are the slow relaxation decays of the single-component samples (indicated by the labels). The corresponding stretched exponential relaxations calculated for the two-component sample are displayed with dashed lines.

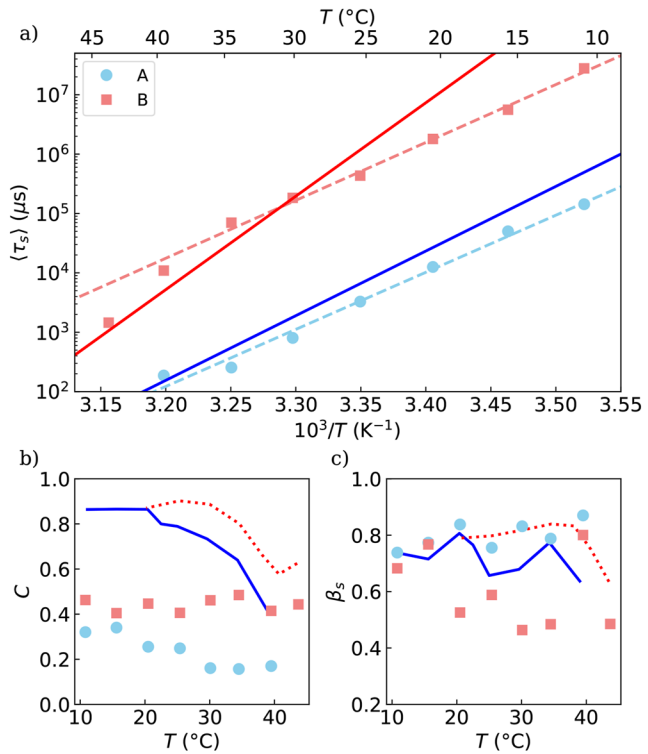


FIG. 7. Fit results for sample AB. (a) T dependence of the average slow relaxation rates (full symbols). The $\langle \tau_s \rangle$ associated with particle A ($\langle \tau_{s,A} \rangle$) is indicated with circles; $\langle \tau_{s,B} \rangle$ values are indicated with squares. The dashed lines are the low- T fits of $\langle \tau_{s,AB} \rangle$ to the Arrhenius law. The Arrhenius fits (full lines) obtained from the single-component samples are shown for comparison using the same color code. The amplitude and stretching exponent of the slow relaxation processes are shown in panels (b) and (c), respectively. The same fit parameters obtained from the single-component samples (solid lines: sample A; dotted lines: sample B) are displayed for comparison.

Arrhenius law, with an activation enthalpy of $\Delta H = -44.6 \text{ kcal/mol}$, a value much lower than the one obtained from the pure B sample (-72 kcal/mol , see Sec. IV A) but quite similar to the one of $\langle \tau_{s,A} \rangle$ (with just a $\sim 1.5\%$ discrepancy).

Apart from the increased noise of the fit, the amplitudes and stretching exponents of the slow relaxation processes [Figs. 7(b) and 7(c)] qualitatively mirror the ones observed in the single-component samples.

We notice that in the binary system, when a sticky end becomes free, it has a small but perhaps not negligible chance of forming transient non-specific bonds with a sticky end of the other component. This, together with the higher NS concentration, could make both networks more fluid and perhaps change the activation enthalpy for the B NSs in the binary system compared to the single-component one. However, we are aware that this reasoning is speculative and more experiments (and possibly detailed simulations with base pair resolution, as in the oxDNA^{27,28} model) are required to properly figure out the origin of the speed-up and of the change in activation enthalpy.

V. DISCUSSION AND CONCLUSIONS

We have shown that a binary mixture of properly designed tetravalent DNA NSs, in which only identical particles can bind to each other, forms on cooling first one network and then, in the remaining empty space, another network at a lower temperature. The two distinct temperatures, at which the two networks form, are controlled by the selected DNA sticky sequences and can thus be tuned by selecting a different number and type of nucleotides in the sticky sequence.

To favor the formation of interpenetrating networks, one needs to make sure that the first-forming network leaves sufficient empty space for the second network to self-assemble. In gels made of DNA NSs, the distance between two bonded NSs (hence, the size of the cavity established around each NS) is essentially controlled by the NS-arm length. To ease this constraint, we have designed ad-hoc the arms of the NS to be composed of 40 bases, twice the size of previously used NSs.⁸ This way, the cavities are large enough to accommodate an additional network.

DLS experiments confirm that the two networks self-assemble sequentially. In general, comparing at constant T the single and double network results, we noticed a weak speed-up of the dynamics of network restructuring in the double network sample. This speed-up indicates that the presence of the other network has a weak but detectable effect on the slow relaxation time. Interestingly, we find that the network relaxation times of the network forming at a lower temperature (i.e., the one with a smaller number of bases in the sticky sequence) retain the same activation enthalpy. This suggests that the presence of the other network modifies mostly the entropic component of the free energy. Instead, when the second network forms, the dynamics of the first forming network not only relaxes faster than in the single network case but also the activation enthalpy is modified, apparently adopting the same activation enthalpy as the companion network.

More studies are needed on this interesting aspect of the dynamics coupling between the two networks.

Finally, we note that three-step decay density-density correlation functions are rarely observed in soft matter systems. Limited evidence is provided by numerical studies of glassy systems close to multiple glass transition critical points.^{33–36} In these cases, as first predicted by mode-coupling-theory,³⁷ the nearby presence of distinct glass lines manifests itself with multiple relaxation times. Here, we have observed a very clear three-step relaxation process, arising in this case from the different time scales of the relaxation processes of the two distinct networks.

ACKNOWLEDGMENTS

This work was supported by the Italian Ministry of Education, University, and Research (MIUR; PRIN 2017—Project No. 2017Z55KCW, Soft Adaptive Networks). Representative images are generated from oxDNA simulations²⁹ using the utility “cogli2.”³⁰ We thank L. Rovigatti for fruitful discussions.

AUTHOR DECLARATIONS

Conflict of Interest

The authors have no conflicts to disclose.

Author Contributions

E. Lattuada: Conceptualization (equal); Formal analysis (equal); Investigation (equal); Methodology (equal); Supervision (equal); Writing – original draft (equal); Writing – review & editing (equal).
T. Pietrangeli: Formal analysis (equal); Investigation (equal).
F. Sciortino: Conceptualization (equal); Formal analysis (equal); Funding acquisition (lead); Methodology (equal); Project administration (lead); Resources (lead); Supervision (equal); Writing – original draft (equal); Writing – review & editing (equal).

DATA AVAILABILITY

The data that support the findings of this study are available within the article.

REFERENCES

- ¹H. Wu, Y. Shen, S. Sivagurunathan, M. S. Weber, S. A. Adam, J. H. Shin, J. J. Fredberg, O. Medalia, R. Goldman, and D. A. Weitz, “Vimentin intermediate filaments and filamentous actin form unexpected interpenetrating networks that redefine the cell cortex,” *Proc. Natl. Acad. Sci. U. S. A.* **119**, e2115217119 (2022).
- ²Y. Shen, H. Wu, P. J. Lu, D. Wang, M. Shayegan, H. Li, W. Shi, Z. Wang, L.-H. Cai, J. Xia *et al.*, “Effects of vimentin intermediate filaments on the structure and dynamics of *in vitro* multicomponent interpenetrating cytoskeletal networks,” *Phys. Rev. Lett.* **127**, 108101 (2021).
- ³L. H. Sperling, *Interpenetrating Polymer Networks and Related Materials* (Springer Science & Business Media, 2012).
- ⁴J. P. Gong, “Why are double network hydrogels so tough?,” *Soft Matter* **6**, 2583–2590 (2010).
- ⁵J.-Y. Sun, X. Zhao, W. R. K. Illeperuma, O. Chaudhuri, K. H. Oh, D. J. Mooney, J. J. Vlassak, and Z. Suo, “Highly stretchable and tough hydrogels,” *Nature* **489**, 133–136 (2012).
- ⁶V. Nigro, B. Ruzicka, B. Ruta, F. Zontone, M. Bertoldo, E. Buratti, and R. Angelini, “Relaxation dynamics, softness, and fragility of microgels with interpenetrated polymer networks,” *Macromolecules* **53**, 1596–1603 (2020).
- ⁷M. Rubinstein and R. Colby, *Polymer Physics* (Oxford University Press, Oxford, 2003).
- ⁸S. Biffi, R. Cerbino, G. Nava, F. Bomboi, F. Sciortino, and T. Bellini, “Equilibrium gels of low-valence DNA nanostars: A colloidal model for strong glass formers,” *Soft Matter* **11**, 3132–3138 (2015).
- ⁹E. Lattuada, D. Caprara, R. Piazza, and F. Sciortino, “Spatially uniform dynamics in equilibrium colloidal gels,” *Sci. Adv.* **7**, eabk2360 (2021).
- ¹⁰F. Bomboi, F. Romano, M. Leo, J. Fernandez-Castanon, R. Cerbino, T. Bellini, F. Bordi, P. Filetici, and F. Sciortino, “Re-entrant DNA gels,” *Nat. Commun.* **7**, 13191 (2016).
- ¹¹N. Conrad, T. Kennedy, D. K. Fygenson, and O. A. Saleh, “Increasing valence pushes DNA nanostar networks to the isostatic point,” *Proc. Natl. Acad. Sci. U. S. A.* **116**, 7238–7243 (2019).
- ¹²F. Bomboi, D. Caprara, J. Fernandez-Castanon, and F. Sciortino, “Cold-swappable DNA gels,” *Nanoscale* **11**, 9691–9697 (2019).
- ¹³E. Stiakakis, N. Jung, N. Adžić, T. Balandin, E. Kentzinger, U. Rücker, R. Biehl, J. K. Dhont, U. Jonas, and C. N. Likos, “Self assembling cluster crystals from DNA based dendritic nanostructures,” *Nat. Commun.* **12**, 7167 (2021).
- ¹⁴B.-j. Jeon, D. T. Nguyen, and O. A. Saleh, “Sequence-controlled adhesion and microemulsification in a two-phase system of DNA liquid droplets,” *J. Phys. Chem. B* **124**, 8888–8895 (2020).
- ¹⁵O. A. Saleh, B.-j. Jeon, and T. Liedl, “Enzymatic degradation of liquid droplets of DNA is modulated near the phase boundary,” *Proc. Natl. Acad. Sci. U. S. A.* **117**, 16160–16166 (2020).
- ¹⁶A. Leathers, M. Walczak, R. A. Brady, A. Al Samad, J. Kotar, M. J. Booth, P. Cicuta, and L. Di Michele, “Reaction-diffusion patterning of DNA-based artificial cells,” *bioRxiv* (2022).

- ¹⁷Y. Sato, T. Sakamoto, and M. Takinoue, "Sequence-based engineering of dynamic functions of micrometer-sized DNA droplets," *Sci. Adv.* **6**, eaba3471 (2020).
- ¹⁸E. Lattuada, M. Leo, D. Caprara, L. Salvatori, A. Stoppacciaro, F. Sciortino, and P. Filetici, "DNA-GEL, novel nanomaterial for biomedical applications and delivery of bioactive molecules," *Front. Pharmacol.* **11**, 01345 (2020).
- ¹⁹S. Walia, V. Morya, A. Gangrade, S. Naskar, A. Guduru Teja, S. Dalvi, P. K. Maiti, C. Ghoroi, and D. Bhatia, "Designer DNA hydrogels stimulate 3D cell invasion by enhanced receptor expression and membrane endocytosis," *ACS Biomater. Sci. Eng.* **7**, 5933–5942 (2021).
- ²⁰M. Leo, E. Lattuada, D. Caprara, L. Salvatori, A. Vecchione, F. Sciortino, P. Filetici, and A. Stoppacciaro, "Treatment of kidney clear cell carcinoma, lung adenocarcinoma and glioblastoma cell lines with hydrogels made of DNA nanostars," *Biomater. Sci.* **10**, 1304–1316 (2022).
- ²¹D. de Las Heras, J. M. Tavares, and M. M. Telo da Gama, "Bicontinuous and mixed gels in binary mixtures of patchy colloidal particles," *Soft Matter* **8**, 1785–1794 (2012).
- ²²F. Seiferling, D. de Las Heras, and M. M. Telo da Gama, "Percolation in binary and ternary mixtures of patchy colloids," *J. Chem. Phys.* **145**, 074903 (2016).
- ²³M. S. Wertheim, "Fluids with highly directional attractive forces. I. Statistical thermodynamics," *J. Stat. Phys.* **35**, 19–34 (1984).
- ²⁴M. S. Wertheim, "Fluids with highly directional attractive forces. II. Thermo-dynamic perturbation theory and integral equations," *J. Stat. Phys.* **35**, 35–47 (1984).
- ²⁵S. Biffi, R. Cerbino, F. Bomboi, E. M. Paraboschi, R. Asselta, F. Sciortino, and T. Bellini, "Phase behavior and critical activated dynamics of limited-valence DNA nanostars," *Proc. Natl. Acad. Sci. U. S. A.* **110**, 15633–15637 (2013).
- ²⁶J. SantaLucia, Jr. and D. Hicks, "The thermodynamics of DNA structural motifs," *Annu. Rev. Biophys. Biomol. Struct.* **33**, 415–440 (2004).
- ²⁷T. E. Ouldridge, A. A. Louis, and J. P. Doye, "Structural, mechanical, and thermodynamic properties of a coarse-grained DNA model," *J. Chem. Phys.* **134**, 085101 (2011).
- ²⁸B. E. Snodin, F. Randisi, M. Mosayebi, P. Šulc, J. S. Schreck, F. Romano, T. E. Ouldridge, R. Tsukanov, E. Nir, A. A. Louis *et al.*, "Introducing improved structural properties and salt dependence into a coarse-grained model of DNA," *J. Chem. Phys.* **142**, 234901 (2015).
- ²⁹The oxDNA program is available at <https://dna.physics.ox.ac.uk>.
- ³⁰Source code is available at <https://sourceforge.net/projects/cogli1/>.
- ³¹B. J. Berne and R. Pecora, *Dynamic Light Scattering: With Applications to Chemistry, Biology, and Physics* (Courier Corporation, 2000).
- ³²F. Bomboi, S. Biffi, R. Cerbino, T. Bellini, F. Bordi, and F. Sciortino, "Equilibrium gels of trivalent DNA-nanostars: Effect of the ionic strength on the dynamics," *Eur. Phys. J. E* **38**, 64 (2015).
- ³³G. Foffi, E. Zaccarelli, P. Tartaglia, F. Sciortino, and K. A. Dawson, "Are particle gels 'glasses'?", in *Trends in Colloid and Interface Science XV* (Springer, 2001), pp. 221–225.
- ³⁴P. Chaudhuri, L. Berthier, P. I. Hurtado, and W. Kob, "When gel and glass meet: A mechanism for multistep relaxation," *Phys. Rev. E* **81**, 040502 (2010).
- ³⁵A. Crisanti and L. Leuzzi, "A simple spin model for three step relaxation and secondary processes in glass formers," *J. Non-Cryst. Solids* **407**, 110–117 (2015).
- ³⁶N. Gnan, G. Das, M. Sperl, F. Sciortino, and E. Zaccarelli, "Multiple glass singularities and isodynamics in a core-softened model for glass-forming systems," *Phys. Rev. Lett.* **113**, 258302 (2014).
- ³⁷W. Götze, *Complex Dynamics of Glass-Forming Liquids: A Mode-Coupling Theory* (Oxford University Press on Demand, 2009), Vol. 143.